PHYSICAL REVIEW C **95**, 062801(R) (2017)

Crust-core transition of a neutron star: Effects of the symmetry energy and temperature under strong magnetic fields

Jianjun Fang, Helena Pais, Sagar Pratapsi, and Constança Providência*
CFisUC, Department of Physics, University of Coimbra, 3004-516 Coimbra, Portugal
(Received 19 April 2017; published 13 June 2017)

We study the simultaneous effects of the symmetry energy and temperature on the crust-core transition of a magnetar. The dynamical and the thermodynamical spinodals are used to calculate the transition region within a relativistic mean-field approach for the equation of state. Quantizing magnetic fields with intensities in the range of $2 \times 10^{15} < B < 5 \times 10^{16}$ G are considered. Under these strong magnetic fields, the crust extension is very sensitive to the density dependence of the symmetry energy, and the properties that depend on the crust thickness could set a constraint on the equation of state. It is shown that the effect on the extension of the crust-core transition is washed out for temperatures above 10^9 K. However, for temperatures below that value, a noticeable effect exists that grows as the temperature decreases and which should be taken into account when the evolution of magnetars is studied.

DOI: 10.1103/PhysRevC.95.062801

Introduction. Magnetars are isolated neutron stars identified as x-ray pulsating sources and soft γ-ray repeaters with very strong surface magnetic fields, $B = 10^{14}$–10^{15} G, and long spin periods ($P = 1$–12 s). Presently, almost 30 magnetars have been identified, see [1,2].

The long term evolution of magnetars has been carried out in Ref. [3]. The authors found that for high values of a temperature independent impurity parameter considered in the upper layers of the inner crust, where according to [4] pasta phases could occur, an enhanced dissipation of the magnetic field is maintained, causing a fast spin down rate of the star. This could be the reason for the nondetection of isolated neutron stars with periods above 12 s. How properties of the pasta phase affect electrical and thermal conductivities is still not clear [5,6].

The crust equation of state (EoS) and its extension, together with the crust-core transition region seem also to play a central role in the evolution of the magnetar magnetic field, in the determination of its configuration [7,8], and in the description of the observed quasiperiodic oscillations (QPO) of soft γ-ray repeaters [9]. Also other crust properties, such as the neutron-drip transition that characterizes the outer-inner crust transition, or the outer-crust structure and composition are affected by strong magnetic fields [10,11].

In [12,13], the effect of strong magnetic fields on the inner crust of neutron stars was discussed within a relativistic mean-field (RMF) model, and several interesting results were obtained. It was found that the inner crust is more complex in the presence of strong magnetic fields, and alternating regions of clusterized and nonclusterized matter appear above the $B = 0$ crust-core transition density. Contrary to the $B = 0$ case, the crust-core transition is defined by a region with a nonzero density width for magnetic fields above $\sim 10^{15}$ G. It was also shown that the width of the transition region is sensitive to the model. This transition region could support the possible existence of highly resistive matter at the upper layers of the inner crust that enhances the decay of the magnetic field.

Neutron star glitches is another phenomenon explained by the crust properties [14]. The crust fractional momentum of inertia is a crucial quantity to interpret glitches. However, recent works have pointed out that due to entrainment effects, that couple the superfluid neutrons to the solid crust, the crust would not be enough to describe glitches [15,16]. The increase of the inner crust due to magnetic field effects found in Refs. [12,13] could validate the crustal contribution to the description of the glitch mechanism.

The cooling of the inner crust of a neutron star occurs more slowly than the core, where a direct Urca process may originate a very fast cooling. During the first years of the star, the cooling of the outer crust, inner crust and core occur independently. It is only when the star is $\sim$50 yr old that its total relaxation has occurred [17]. The temperature of the crust depends on the star mass and on the EoS, but a newly born star, less than one year old, will have a temperature above 10^9 K. At the star's total relaxation, the temperature has dropped well below $\sim 10^9$ K. Moreover, the magnetic field and temperature evolutions are strongly coupled in a neutron star which require coupled magneto-thermal evolution to properly study the star cooling [18–20]. It is, therefore, of interest to study how sensitive is the increase of the crust-core transition region to temperature.

In the present study, we will use RMF models [21], which are phenomenological models constrained by different types of observables, in particular, experimental measurements, theoretical *ab initio* calculations and observations in astronomy, see [22] for a review. Taking a set of models that have the same isoscalar properties at saturation, and only differ on the isovector properties, will allow to investigate how the effect of the magnetic field on the stellar matter depends on the properties of the EoS, in particular, on the density dependence of the symmetry energy.

First we analyze the effect of the density dependence of the symmetry energy on the magnetar crust-core transition within the dynamical spinodal formalism at zero temperature. Next,

*cp@fis.uc.pt

the effect of temperature is studied. This will be done using the finite temperature thermodynamical spinodal [23,24], and temperatures between 1 and 1000 keV (10^7–10^{10} K). Although the crust-core transition density is ∼10% larger in the thermodynamical spinodal approach, as compared to the dynamical one, see [25,26], we believe it will allow us to perform a realistic discussion. The same approach was used at zero temperature to study the liquid-gas phase transition of magnetized nuclear matter in [27,28].

Formalism. Stellar matter is described within the nuclear RMF formalism under the effect of strong magnetic fields [28,29]. The anomalous magnetic moment (AMM) is included in part of the calculations. The nuclear interaction is described through the inclusion of mesonic fields: an isoscalar-scalar field ϕ with mass m_s, an isoscalar-vector field V^μ with mass m_v, and an isovector-vector field $\mathbf{b}^\mu$ with mass m_ρ. Besides nucleons with mass m, electrons with mass m_e are also included in the Lagrangian density. Protons and electrons interact through the electromagnetic field A^μ, which includes a static component assumed to be externally generated, $A^\mu = (0,0,Bx,0)$, so that $\mathbf{B} = B\,\hat{z}$ and $\nabla\cdot\mathbf{A} = 0$. We take the usual RMF Lagrangian density $\mathcal{L} = \sum_{i=p,n}\mathcal{L}_i + \mathcal{L}_e + \mathcal{L}_\sigma + \mathcal{L}_\omega + \mathcal{L}_\rho + \mathcal{L}_{\omega\rho} + \mathcal{L}_A$, where $\mathcal{L}_i$ is the nucleon Lagrangian density, given by

$$\mathcal{L}_i = \bar{\psi}_i\left[\gamma_\mu i D^\mu - M_i^* - \tfrac{1}{2}\mu_N\kappa_b\sigma_{\mu\nu}F^{\mu\nu}\right]\psi_i$$

with $iD^\mu = i\partial^\mu - g_v V^\mu - \frac{g_\rho}{2}\boldsymbol{\tau}\cdot\mathbf{b}^\mu - eA^\mu\frac{1+\tau_3}{2}$, $M_p^* = M_n^* = M^* = m - g_s\phi$, and the mesonic and photonic terms defined as in [13]. The term $\mathcal{L}_{\omega\rho} = \Lambda_v g_v^2 g_\rho^2 V_\mu V^\mu \mathbf{b}_\mu\cdot\mathbf{b}^\mu$ couples the ρ to the ω meson and allows the softening of the density dependence of the symmetry energy above saturation density [30,31]. We consider the NL3 [32] and NL3$\omega\rho$ [30,31] parametrizations, which describe two solar mass stars [33]. The last ones are obtained from the NL3 model by including the $\omega\rho$ term. All models have the same isoscalar properties at saturation, in particular, the binding energy $E_b = -16.2$ MeV, the saturation density $\rho_0 = 0.148$ fm^{-3}, and the incompressibility $K = 272$ MeV. The isovector properties, such as the symmetry energy and its slope L at saturation, vary from model to model, and have been fixed such that, at $\rho = 0.1$ fm^{-3}, all models have the same symmetry energy, $\epsilon_{sym}(0.1) = 25.7$ MeV. Besides NL3 with $L = 118$ MeV, we also take NL3$\omega\rho$ with $L = 88$, 68, and 55 MeV. The model with $L = 55$ MeV satisfies the constraints imposed by microscopic calculations of neutron matter [34]. The nucleon AMM is introduced via the coupling of the baryons to the electromagnetic field tensor with $\sigma_{\mu\nu} = \frac{i}{2}[\gamma_\mu,\gamma_\nu]$, and strength κ_b with $\kappa_n = -1.91315$ for the neutron, and $\kappa_p = 1.79285$ for the proton. μ_N is the nuclear magneton. We will not consider the AMM of the electrons because its contribution is negligible for the magnetic field intensities we consider in the present work [35].

The state which minimizes the energy of asymmetric *npe* matter is characterized by the distribution functions $f_{0i\pm} = [1 + e^{(\epsilon_{0i}\mp\nu_i)/T}]^{-1}$ with $\nu_i = \mu_i - g_v V_0 - \frac{g_\rho}{2}\tau_i b_0$ for $i = p,n$, and $\nu_e = \mu_e$ for the electrons, and by the constant mesonic fields which obey the mesonic equations [13]. For $T = 0$ MeV, the distribution functions $f_{0i\pm}$ become $f_{0i+} = \theta(P_{Fi}^2 - p^2)$, $f_{0i-} = 0$ [36].

Nuclear matter at subsaturation densities has a liquid-gas phase transition. Homogeneous matter is unstable if the free energy curvature is negative. The stability conditions for asymmetric nuclear matter are obtained from the free energy density, by imposing that the function is convex on the densities ρ_p and ρ_n, keeping the volume and temperature constant [23]. The thermodynamical spinodal is the surface in the (ρ_n, ρ_p, T) space where the determinant of the free energy curvature matrix is zero. Inside this surface, nuclear matter is unstable.

Symmetry energy effect. We first discuss the effect of the symmetry energy on the crust-core transition. The density and the proton fraction of the crust-core transition in a neutron star are functions of the density dependence of the symmetry energy. In particular, they are correlated with the slope L of the symmetry energy at saturation [25,26,37–39]. We may, therefore, expect that the effect of a strong magnetic field on the transition will also depend on the symmetry energy, since the magnetic field is sensitive to the amount of protons: the smaller the proton density, the stronger are the effects. In previous studies [12,13], this aspect has already been identified.

Within the dynamical spinodal formalism presented in [13], we determine the maximum growth rates Γ as a function of the density, using the $B = 0$ proton fraction (y_p^0) below the crust core transition and, above it, the β-equilibrium proton fraction. Thomas-Fermi (TF) calculations of the inner crust indicate that from $\rho \sim 0.01$ fm^{-3} up to the crust-core transition density, which at $B = 0$ we designate by ρ_t^0, the proton fraction does not change much [40]. Unlike the case for $B = 0$, there is no well defined transition density for a strong magnetic field, but a sequence of unstable and stable regions ranging from ρ_1—defined, as in [13], as the first time the growth rate falls to zero, which is smaller than but close to ρ_t^0—up to ρ_2—the onset of the homogenous matter, taking the proton fraction of β-equilibrium matter. Both densities coincide with ρ_t^0 at $B = 0$.

The four models introduced above have the same isoscalar properties, but a different density dependence of the symmetry energy. In Fig. 1, we show, as a function of the slope L: a) the densities that define the beginning and the end of the transition region, ρ_1 and ρ_2 (a); b) the thickness of the crust calculated with ρ_2, $\Delta R = R(0) - R(\rho_2)$, and with ρ_1, $\Delta R^* = R(0) - R(\rho_1)$ (b); and c) the crust fractional moment of inertia, $\Delta I_{cr}/I$, using the approximate expression [41]

$$\frac{\Delta I_{cr}}{I} \simeq \frac{28\pi P_t R^3}{3M}\frac{(1 - 1.67\beta - 0.6\beta^2)}{\beta} \times\left[1 + \frac{2P_t(1 + 5\beta - 14\beta^2)}{\rho_t m\beta^2}\right]^{-1}, \quad (1)$$

and taking for the transition density ρ_t and pressure P_t the limiting densities of the transition density, (ρ_2, P_2) and (ρ_1, P_1) (c). In this expression, ΔI_{cr} is the crust moment of inertia, I is the total moment of inertia of the star, M and R are the gravitational mass and radius of the star, $\beta = GM/R$ is the compactness parameter, and m is the nucleon mass. The quantities in Fig. 1 are calculated at $T = 0$ for $B^* = 10^3$ and $L = 55$ from the dynamical spinodal formalism with AMM.

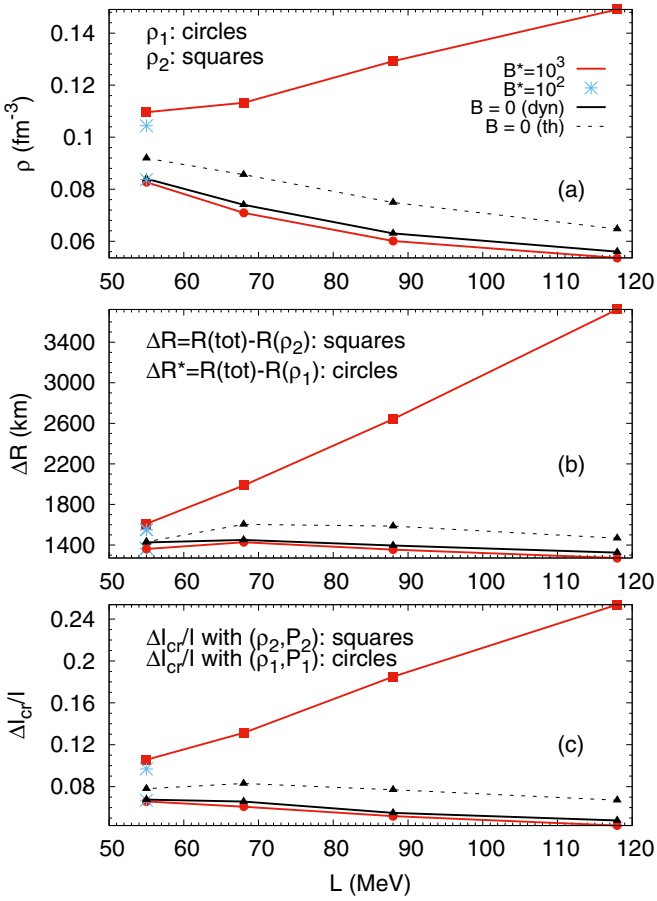

FIG. 1. Transition densities, ρ_1 and ρ_2 (a) the crust thickness, ΔR and $\Delta R^* = R(\mathrm{tot}) - R(\rho_1)$ (b) the crust fractional momentum of inertia, calculated with (ρ_1, P_1) and with (ρ_2, P_2) (c) versus the symmetry energy slope L, obtained at $T = 0$ with $B^* = 10^3$ (red) and $B = 0$ (black solid), within the dynamical spinodal formalism including the AMM. For $L = 55$ MeV also $B^* = 10^2$ is shown (blue stars). $B = 0$ results from the thermodynamical spinodal calculation are also included (black dashed).

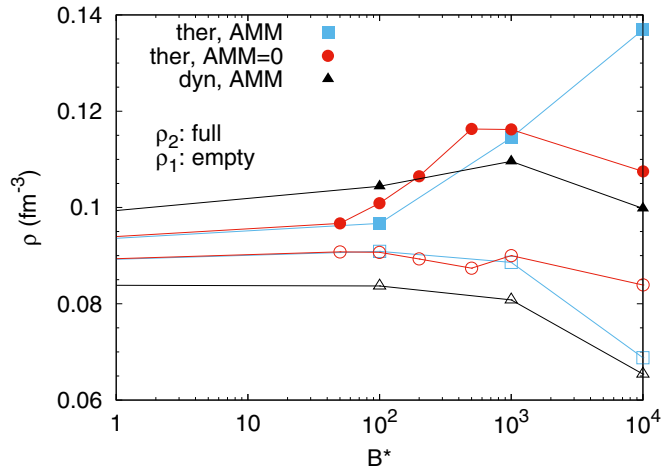

FIG. 2. The transition densities, ρ_1 (empty) and ρ_2 (full) obtained with the $L = 55$ MeV model, at $T = 0$, for several values of B^*, and using the thermodynamical spinodal formalism with (squares) and without AMM (circles), and the dynamical spinodal with AMM (triangles).

The blue stars are for $B^* = 10^2$. For $B = 0$, we include the results from a dynamical and a thermodynamical spinodal calculation, respectively, with and without AMM.

The effect of B and L on the thickness of the crust is summarized in the following: a) the larger the L, the larger the effect of B, mainly due to the proton fraction associated with each model, since a larger L is associated with a smaller proton fraction; b) compared to $B = 0$, the effect can be as large as a 100% for $L = 118$ MeV. However, experimental constraints [42] and microscopic neutron matter calculations [34] indicate that the models with $L = 30$–80 MeV are more realistic. For $L = 55$ MeV, the effect corresponds to an increase of ∼20%; c) the lower limit of the crust-core transition defined by ρ_1 is just slightly smaller than the $B = 0$ crust-core transition ρ_t^0. The magnetic field essentially creates a complex transition region above this density; d) taking $L = 55$ MeV and decreasing the magnetic field by an order of magnitude from $B^* = 10^3$ to $B^* = 10^2$, quantities such as the transition density, the crust thickness and the crust fraction of moment of inertia, defined with the density ρ_2, suffer a reduction of ∼3–5 %, but are still larger than the corresponding quantities at $B = 0$. We conclude by stressing that properties of magnetized neutron stars that directly depend on the thickness of the crust may set stringent constraints on the symmetry energy slope L.

Temperature effect. We estimate the effect of temperature on the crust transition by calculating the thermodynamical spinodal of strongly magnetized nuclear matter. In Ref. [24], it has been shown that due to the large incompressibility of the electron gas, most models that describe *npe* matter do not present thermodynamical instabilities, or present only a very reduced region of instabilities. Thermodynamical stability does not necessary mean that the *npe* system is stable to small density fluctuations, as shown in [36,43,44]. Calculating the dynamical spinodal determines precisely the instability region taking into account the independent fluctuations of the neutron, proton, and electron densities. However, according to [26,45], the *np* matter thermodynamical spinodal gives a good prediction of the crust-core transition density, just slightly above the prediction from a TF calculation or a dynamical spinodal for *npe* matter. This behavior is confirmed in Fig. 1 where the $B = 0$ quantities determined from the dynamical and the thermodynamical spinodals have been plotted. The values predicted from the thermodynamical spinodal are always ∼15% larger than the ones from the dynamical spinodal. For a strong magnetic field with an intensity of the order we have considered in this work, the effect is similar. In Fig. 2, we plot the crust-core transition densities, ρ_1 and ρ_2, obtained at $T = 0$ with the $L = 55$ MeV model from the *npe* dynamical spinodal with AMM, and from the *np* thermodynamical spinodals with and without AMM, to estimate the limitations of our predictions. The lower (upper) density ρ_1 (ρ_2) corresponds to the density where the β-equilibrium EoS first (last) crosses the spinodal, see Fig. 3.

Comparing the results obtained from the dynamical and thermodynamical spinodals we conclude the following: a)

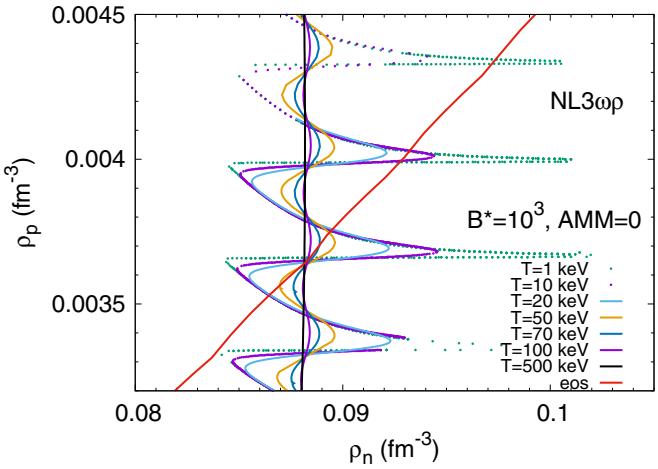

FIG. 3. Details of the crossing of the thermodynamical spinodal with the EoS (black solid line) for NL3$\omega\rho$ with $B^* = 10^3$, considering different temperatures, and taking AMM = 0.

the dynamical and thermodynamical spinodals predict the same trends for the transition densities, though the dynamical spinodal predicts smaller values of ρ_1, in accordance with results from [26,45]. However, for the upper limit of the transition region, there is a dependence on B, and the dynamical ρ_2 is larger (smaller) than the thermodynamical one for $B^* < 10^2$ ($B^* > 10^2$); b) AMM does not affect much the results obtained with $B^* < 10^3$. However, the AMM reduces in a non-negligible way the instability region for the larger fields, giving rise to smaller crust thicknesses and momentum of inertia crustal fractions.

The temperature of the crust decreases as the star cools. While a very young star, less than one year old, may have a inner crust temperature above 10^9 K, it will drop below 10^9 K, or even 10^8 K, depending on the EoS considered and the mass of the star [17,46]. It is, therefore, reasonable to ask whether the strong effect of the magnetic field on the crust-core transition calculated at $T = 0$, with the appearance of a transition region where stable and unstable regions alternate, still persists at finite temperature. Moreover, the time evolution of both the magnetic field and temperature inside the star are strongly coupled, and, therefore, it is important to understand which is the effect of the temperature on the transition region created by a magnetic field.

We calculate the crust-core transition density/region for temperatures in the range 1 keV $< T <$ 1 MeV ($10^7 \lesssim T \lesssim 10^{10}$ K) from the thermodynamical spinodal without AMM. Above $B^* \sim 10^3$ ($B \sim 5 \times 10^{16}$ G), the AMM has a non-negligible effect and, therefore, we will essentially restrict ourselves to values below that number. As discussed in [12,13], the spinodal section shows a complex structure and bands of instability with large isospin asymmetry appear associated with the filling of the different Landau levels. As a result for low temperatures, the β-equilibrium EoS crosses the spinodal section several times, defining the region of instability referred before, see Fig. 3. The transition region for $T = 10$ keV is smaller than for $T = 1$ keV since the EoS is not crossing the last band shown. The transition region decreases as T increases

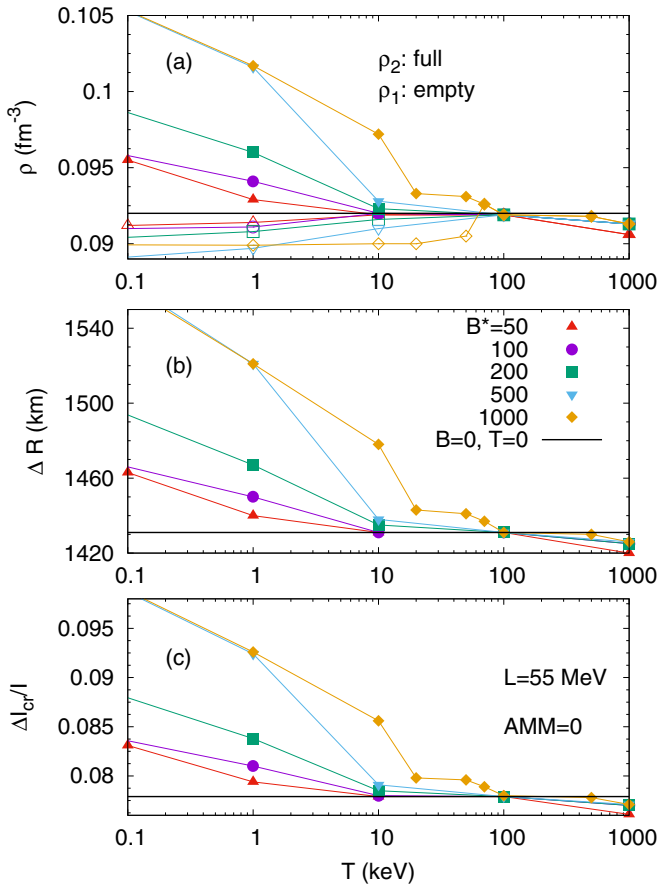

FIG. 4. The transition densities, ρ_1 (empty) and ρ_2 (full), (a), the crust thickness (b), and the momentum of inertial crustal fraction (c) for NL3$\omega\rho$, with $L = 55$ MeV, for several values of B^* and T.

and, for large enough temperatures, the crossing occurs at a well defined density, as for $T \geqslant 100$ keV in Fig. 3. The Landau quantization will be completely washed out by temperatures of the order of the energy separation between consecutive Landau levels, i.e., $T \gtrsim eB/M^* = m_e^2 B^*/M^*$. For $B^* = 1000$ and taking $M^* \sim 700$ MeV for $\rho \sim 0.09$ fm^{-3}, this corresponds to $T \gtrsim 0.3$ MeV. The effects become important already for 10% of this value in the regions of larger isospin asymmetry, e.g., larger ρ_n.

We plot in Fig. 4 the transition densities, ρ_1 and ρ_2 (a), the crust thickness, ΔR (b), and the momentum of inertia crustal fraction (c) for $B^* \leqslant 10^3$ and $10^{-1} \leqslant T \leqslant 10^3$ keV. These quantities together with the corresponding transition pressures are given in the Supplemental Material [47]. The crust thicknesses are estimated from the Tolmann-Oppenheimer-Volkoff (TOV) equations [48] at $B = 0$. The densities ρ_2 come closer to the lower limit, ρ_1, of the transition region as the temperature increases, and for the magnetic field intensities considered, all magnetic field effects have been washed out at $T = 100$ keV, and the $B = 0$ transition density has been recovered. For a stronger field, this is not anymore true, but since for these stronger fields, several of the suppositions considered in the present work break, such as the use of the TOV equations or the exclusion of the AMM of the nucleons,

we will not discuss so strong fields. Above $T = 100$ keV, ρ_1 and ρ_2 coincide, but they take values below the $T = 0$ transition density: this is the reduction of the extension of the spinodal section due to temperature effects. To summarize, we may expect the appearance of a transition region with nonzero thickness for crustal temperatures below 100 keV and a magnetic field intensity at the crust-core transition below $B \sim 5 \times 10^{16}$ G.

Also, the crust momentum of inertia fraction is affected, and is large enough to account for the Vela glitches, which, and according to [16], would require a fractional crustal momentum of inertia of the order of ∼0.065–0.095, considering that the effective neutron mass, including entrainment effects, is 4–6 times larger than the neutron bare mass. However, further studies should be undertaken because strong magnetic fields as the ones considered in the present work will certainly influence the neutron superfluid behavior and affect the neutron entrainment to the lattice.

The main effect of having used the thermodynamical spinodal instead of the dynamical one is that the predicted crust-core transition density is ∼10% larger, the crust fraction momentum of inertia ∼10–15 % larger, and the transition region slightly smaller, but the overall conclusions remain valid.

Conclusion. We have analyzed how the effects of a strong magnetic field on the neutron star crust, previously studied in [12,13], are affected by the density dependence of the symmetry energy of the EoS, and by the temperature of the crust, within a RMF description of *npe* and *np* matter. At $T = 0$, the crust-core transition was obtained from the dynamical spinodal with AMM, and at finite temperatures, from the thermodynamical spinodal, excluding the AMM, which is justified since only magnetic fields below 5×10^{16} G are considered.

We have confirmed the results of Refs. [12,13]: due to the sensitivity of the magnetic field to the proton density, the extension of the crust-core transition region strongly depends on the slope L of the symmetry energy. The larger the slope L, the larger the transition region, because, below saturation density, models with a large L present smaller symmetry energies and, therefore, accept smaller proton fractions. Experimental and theoretical constraints seem to limit L below 80 MeV ($30 < L < 80$ MeV) [42], resulting in a more moderate effect of the magnetic field on the extension of the crust. Properties of magnetized neutron stars that directly depend on the thickness of the crust can set stringent constraints on the symmetry energy slope L due to the great sensitivity of the crust size to this property.

We have also studied the effect of temperature for magnetic fields $B \leqslant 5 \times 10^{16}$ G. The magnetic field effects on the extension of the transition density are washed out for temperatures above 10^9 K, but below these temperatures, even a field of intensity 2×10^{15} G will have a finite effect on the crust thickness. Microphysical parameters, such as transport coefficients, that enter in the magneto-thermal evolution equations of a neutron star, are certainly affected by the existence of the crust-core transition region that changes with cooling, and the impact of this effect should be investigated. Recently, a one-dimensional thermal-magneto-plastic model, that considered transport coefficients sensitive to temperature, as well as the coupling of the crustal motion to the magnetosphere, has been implemented, and it has been shown that this coupling induces an enrichment and acceleration of the magnetar dynamics [49].

Acknowledgments. This work is partly supported by the FCT (Portugal) Project No. UID/FIS/04564/2016, and by "NewCompStar", COST Action MP1304. H.P. is supported by FCT (Portugal) under Project No. SFRH/BPD/95566/2013.

[1] S. A. Olausen and V. M. Kaspi, Astrophys. J. Suppl. Ser. **212**, 6 (2014).
[2] SGR/APX online catalogue, http://www.physics.mcgill.ca/∼pulsar/magnetar/main.html.
[3] J. A. Pons, D. Viganò, and N. Rea, Nat. Phys. **9**, 431 (2013).
[4] D. G. Ravenhall, C. J. Pethick, and J. R. Wilson, Phys. Rev. Lett. **50**, 2066 (1983).
[5] C. J. Horowitz, D. K. Berry, C. M. Briggs, M. E. Caplan, A. Cumming, and A. S. Schneider, Phys. Rev. Lett. **114**, 031102 (2015).
[6] D. G. Yakovlev, Mon. Not. R. Astron. Soc. **453**, 581 (2015).
[7] S. K. Lander, Mon. Not. R. Astron. Soc. **437**, 424 (2014).
[8] S. K. Lander, Astrophys. J. Lett. **824**, L21 (2016).
[9] M. Gabler, P. Cerdá-Durán, N. Stergioulas, J. A. Font, and E. Müller, Phys. Rev. Lett. **111**, 211102 (2013).
[10] N. Chamel, Z. K. Stoyanov, L. M. Mihailov, Y. D. Mutafchieva, R. L. Pavlov, and C. J. Velchev, Phys. Rev. C **91**, 065801 (2015).
[11] D. Basilico, D. P. Arteaga, X. Roca-Maza, and G. Colò, Phys. Rev. C **92**, 035802 (2015).
[12] J. Fang, H. Pais, S. S. Avancini, and C. Providência, Phys. Rev. C **94**, 062801(R) (2016).
[13] J. Fang, H. Pais, S. Pratapsi, S. Avancini, J. Li, and C. Providência, Phys. Rev. C **95**, 045802 (2017).
[14] B. Link, R. I. Epstein, and J. M. Lattimer, Phys. Rev. Lett. **83**, 3362 (1999).
[15] N. Chamel, Phys. Rev. C **85**, 035801 (2012); Phys. Rev. Lett. **110**, 011101 (2013).
[16] N. Andersson, K. Glampedakis, W. C. G. Ho, and C. M. Espinoza, Phys. Rev. Lett. **109**, 241103 (2012).
[17] D. G. Yakovlev, A. D. Kaminkera, O. Y. Gnedinc, and P. Haensel, Phys. Rep. **354**, 1 (2001).
[18] D. N. Aguilera, J. A. Pons, and J. A. Miralles, Astron. Astrophys. **486**, 255 (2008).
[19] D. Viganò and J. A. Pons, Mon. Not. R. Astron. Soc. **425**, 2487 (2012).
[20] D. Viganò, N. Rea, J. A. Pons, R. Perna, D. N. Aguilera, and J. A. Miralles, Mon. Not. R. Astron. Soc. **434**, 123 (2013).
[21] B. D. Serot and J. D. Walecka, Adv. Nucl. Phys. **16**, 1 (1986); J. Boguta and A. R. Bodmer, Nucl. Phys. A **292**, 413 (1977).
[22] M. Oertel, M. Hempel, T. Klähn, and S. Typel, Rev. Mod. Phys. **89**, 015007 (2017).
[23] J. Margueron and P. Chomaz, Phys. Rev. C **67**, 041602(R) (2003).
[24] S. S. Avancini, L. Brito, P. Chomaz, D. P. Menezes, and C. Providência, Phys. Rev. C **74**, 024317 (2006).

[25] C. Ducoin, J. Margueron, and C. Providência, Eur. Phys. Lett. **91**, 32001 (2010).
[26] C. Ducoin, J. Margueron, C. Providência, and I. Vidaña, Phys. Rev. C **83**, 045810 (2011).
[27] Y. J. Chen, Phys. Rev. C **95**, 035807 (2017).
[28] A. Rabhi, C. Providência, and J. d. Providência, J. Phys. G: Nucl. Part. Phys. **35**, 125201 (2008).
[29] A. Broderick, M. Prakash, and J. M. Lattimer, Astrophys. J. **537**, 351 (2000).
[30] C. J. Horowitz and J. Piekarewicz, Phys. Rev. Lett. **86**, 5647 (2001); Phys. Rev. C **64**, 062802 (2001).
[31] H. Pais and C. Providência, Phys. Rev. C **94**, 015808 (2016).
[32] G. A. Lalazissis, J. König, and P. Ring, Phys. Rev. C **55**, 540 (1997).
[33] M. Fortin, C. Providência, A. R. Raduta, F. Gulminelli, J. L. Zdunik, P. Haensel, and M. Bejger, Phys. Rev. C **94**, 035804 (2016).
[34] K. Hebeler, J. M. Lattimer, C. J. Pethick, and A. Schwenk, Astrophys. J. **773**, 11 (2013); S. Gandolfi, J. Carlson, and S. Reddy, Phys. Rev. C **85**, 032801 (2012).
[35] R. C. Duncan, AIP Conf. Proc. **526**, 830 (2000).
[36] L. Brito, C. Providência, A. M. Santos, S. S. Avancini, D. P. Menezes, and P. Chomaz, Phys. Rev. C **74**, 045801 (2006).
[37] I. Vidaña, C. Providência, A. Polls, and A. Rios, Phys. Rev. C **80**, 045806 (2009).
[38] J. Xu, L. W. Chen, B. A. Li, and H. R. Ma, Astrophys. J. **697**, 1549 (2009).
[39] W. G. Newton, M. Gearheart, and B. A. Li, Astrophys. J. Suppl. Ser. **204**, 9 (2013).
[40] F. Grill, C. Providência, and S. S. Avancini, Phys. Rev. C **85**, 055808 (2012).
[41] J. M. Lattimer and M. Prakash, Phys. Rep. **333**, 121 (2000).
[42] M. B. Tsang, J. R. Stone, F. Camera, P. Danielewicz, S. Gandolfi, K. Hebeler, C. J. Horowitz, J. Lee, W. G. Lynch, Z. Kohley, R. Lemmon, P. Möller, T. Murakami, S. Riordan, X. Roca-Maza, F. Sammarruca, A. W. Steiner, I. Vidaña, and S. J. Yennello, Phys. Rev. C **86**, 015803 (2012).
[43] C. J. Pethick, D. G. Ravenhall, and C. P. Lorenz, Nucl. Phys. A **584**, 675 (1995).
[44] C. Providência, L. Brito, S. S. Avancini, D. P. Menezes, and P. Chomaz, Phys. Rev. C **73**, 025805 (2006).
[45] S. S. Avancini, S. Chiacchiera, D. P. Menezes, and C. Providência, Phys. Rev. C **82**, 055807 (2010).
[46] N. Chamel and P. Haensel, Living Rev. Relativity **11**, 10 (2008).
[47] See Supplemental Material at http://link.aps.org/supplemental/10.1103/PhysRevC.95.062801 for the transition densities and pressures, crust thicknesses, and the correspondent fractional crustal moment of inertia obtained from a thermodynamical spinodal calculation without AMM and $L = 55$ MeV, for a star of $M = 1.4 M\odot$ and $R = 13.734$ km.
[48] R. C. Tolman, Phys. Rev. **55**, 364 (1939); J. R. Oppenheimer and G. M. Volkoff, *ibid.* **55**, 374 (1939).
[49] X. Li, Y. Levin, and A. M. Beloborodov, Astrophys. J. **833**, 189 (2016).